ELECTRORHEOLOGICAL DAMPER WITH ANNULAR DUCTS FOR SEISMIC PROTECTION APPLICATIONS

by

Nicos Makris
Department of Civil and Environmental Engineering
University of California at Berkeley
Berkeley, CA 94720

Scott A. Burton
Department of Civil Engineering and Geological Sciences
University of Notre Dame
Notre Dame, IN 46556

Douglas P. Taylor
Taylor Devices, Inc.
90 Taylor Drive
North Tonawanda, NY 14120

Smart Mater. Struct. 5 (1996) 551–564. Printed in the UK

Electrorheological damper with annular ducts for seismic protection applications

Nicos Makris†, Scott A Burton‡ and Douglas P Taylor§

† Department of Civil and Environmental Engineering, University of California at Berkeley, Berkeley, CA 94720, USA
‡ Department of Civil Engineering and Geological Sciences, University of Notre Dame, Notre Dame, IN 46556, USA
§ Taylor Devices Inc., 90 Taylor Drive, North Tonawanda, NY 14120, USA

Received 23 April 1996, accepted for publication 27 July 1996

Abstract. This paper presents the design, analysis, testing and modeling of an electrorheological (ER) fluid damper developed for vibration and seismic protection of civil structures. The damper consists of a main cylinder and a piston rod that pushes an ER fluid through a stationary annular duct. The behavior of the damper can be approximated with Hagen–Poiseuille flow theory. The basic equations that describe the fluid flow across an annular duct are derived. Experimental results on the damper response with and without the presence of electric field are presented. As the rate of deformation increases, viscous stresses prevail over field-induced yield stresses and a smaller fraction of the total damper force can be controlled. Simple physically motivated phenomenological models are considered to approximate the damper response with and without the presence of electric field. Subsequently, the performance of a multilayer neural network constructed and trained by an efficient algorithm known as the Dependence Identification Algorithm is examined to predict the response of the electrorheological damper. A combination of a simple phenomenological model and a neural network is then proposed as a practical tool to approximate the nonlinear and velocity-dependent damper response.

1. Introduction

Conventional seismic design of buildings and bridges relies on the ability of structures to behave inelastically and dissipate the induced seismic energy through hysteretic action. Most structures absorb earthquake energy through localized damage of their supporting members. During the last two decades considerable advances have been accomplished in the area of seismic protection of structures due to developments in base isolation and supplemental energy dissipation. New promising systems have been developed which can be incorporated in structures to improve their response when excited by earthquakes (ATC 1993). These systems also known as earthquake protective systems consist of passive, active and semiactive devices and can considerably minimize the seismic demand of buildings and bridges.

Semi-active dampers for retrofit and vibration control of structures combine the advantages of passive structural control (Constantinou and Symans 1993) with the benefits of active structural control (Housner *et al* 1994) to produce optimal, yet stable and reliable damping systems. Different types of semi-active dampers have been proposed ranging from hydraulic dampers with mechanically controlled orificing (Kawashima and Unjoh 1994, Patten *et al* 1994, Symans and Constantinou 1995) to electrorheological dampers (Gavin and Hanson 1994a, b, Burton *et al* 1996, Makris *et al* 1996).

The attraction of semiactive dampers that use controllable fluids such as electrorheological (ER) or magnetorheological (MR) fluids is that they do not involve moving parts to control the fluid flow. Furthermore, they are relatively inexpensive compared with hydraulic dampers with mechanically controlled orificing. A survey on the applications of ER fluids has been presented by Duclos (1988), and recently by Stanway *et al* (1996).

Within the context of structural control, Ehrgott and Masri (1992) presented identification techniques to model the behavior of a small ER damper that operates under shear flow; Gavin and Hanson (1994a, b) designed and tested an ER damper that consists of a rectangular container and a moving plunger comprising nine flat parallel plates which are rigidly interconnected.

A prototype ER damper that generates flow through a stationary annular duct was designed constructed and tested by the authors (Burton *et al* 1996, Makris *et al* 1996). The proposed ER damper can deliver relatively large forces and has potential to be used for seismic and vibration protection

0964-1726/96/050551+14$19.50

of civil structures. A photograph of the constructed damper is shown in figure 1 (top), and a schematic of its design is shown in figure 1 (bottom). The damper consists of an outer cylinder and a double-ended piston rod that pushes the ER fluid through stationary annular ducts. The electric field is created perpendicular to the fluid flow.

In this paper we first present the equations that approximate the flow of a controllable fluid when it flows through a stationary annular duct. These equations are important for the design and size of the damper, since they relate the pressure drop across the piston head to the piston velocity, the physical properties of the ER fluid and the geometric characteristics of the damper. The validity of these equations is investigated by comparing their prediction with the measured response of the ER damper. Subsequently, we investigate the effectiveness of parametric and nonparametric macroscopic models which approximate the damper response at the force–displacement level. In particular it is shown that the combination of a two-parameter Maxwell model with a neural network is an effective model to approximate the nonlinear and velocity-dependent response of the proposed ER damper.

2. Viscous, rigid-viscoplastic and elastic-viscoplastic behavior

In this section the flow across an annular duct is reviewed for fluids described by different constitutive laws. Figure 2 shows a cross section of the annular duct that consists of the inner rod (electrode) and the outer cylinder (ground). Under the condition that laminar flow prevails, the flow along the bypass can be approximated by the Hagen–Poiseille theory. Laminar flow occurs in practice when the Reynolds number, $R = \bar{v}h/\nu$ ($\bar{v}$ = average velocity of the fluid in the duct, h = characteristic length, ν = kinematic viscosity) has a value less than, $R_{crit} = 2300$. Since the flow rate across the bypass is $Q = v_p A_p/n$ (v_p = piston velocity, A_p = piston area, n = number of bypasses—in this case $n = 1$); the Reynolds number for the flow along the ER duct with $h \ll d$, is

$$R_e = \frac{\bar{v}h}{\nu} = \frac{Q}{\pi d \nu}. \tag{1}$$

When ER dampers are incorporated in the skeleton of a building for seismic retrofit, the expected Reynolds number assumes values smaller than ten ($R_e < 10$, Makris *et al* 1996). Accordingly, since the Reynolds number is two to three orders of magnitude less than R_{crit}, the flow within the damper is laminar.

Equation (1) was derived for viscous flow across a thin annular duct in which $h \ll d$ (see figure 2). In this case the area of the duct is πdh. When an electric field is applied, the material exhibits a yield stress and part of the material moves as a rigid body without deforming. In this case, the characteristic dimension is less than h, and the Reynolds number reduces further (Phillips 1969). Accordingly, the viscous forces and inertia forces developed within the fluid are of the same order of magnitude.

With reference to figure 2 one can easily show by considering equilibrium of any ring of the material, that under the absence of inertia forces, the distribution of stresses across the bypass is linear and given by

$$\tau_{xr}(r) = \Delta p \frac{r}{L} \tag{2}$$

where Δp is the pressure drop across the piston head, r is the radial distance from the center line of the ER duct, and L is the length of the duct (see figure 1). The stress distribution given by (2) is independent of the material that flows. In the case where $h \ll d$, the solution for the Poiseille flow between concentric cylinders collapses to that for flow between parallel plates.

2.1. Flow of viscous fluid

For a viscous fluid with zero-shear-rate viscosity, ν_0, the shear stress–strain law is

$$\tau_{xr} = \nu_0 \dot{\gamma}_{xr} \tag{3}$$

where $\dot{\gamma}_{xr}$ is the shear strain rate. The pressure drop due to viscous stresses under steady flow is given by

$$\Delta p_v = \frac{12 \nu_0 L Q}{\pi d h^3}. \tag{4}$$

For oscillatory flow, the pressure drop is influenced by the inertia of the fluid. The complete solution for flow through an annular circular cross section has been presented by Müller (1936). The pressure drop generated from the accelerating flow departs from the result given by (4) only at very high fluid accelerations, which are not of interest in earthquake engineering.

2.2. Flow of viscoplastic material

The phenomenon of electrorheology was first reported by Winslow (1949) and is the considerable variation of rheological properties of some fluids when an electric field is applied. The manifested resistance to flow depends on the nature of the fluid, the conditions of flow and the orientation and strength of the applied electric field. In some cases complete conversion from liquid to solid behavior is achieved for which a finite yield stress, τ_y, must be exceeded to produce flow. When the latter is the case, it can be said that under the presence of an electric field these 'fluids' become 'solids', and they behave elastically when loaded at stresses smaller than the 'yield' stress. Recent reviews on the phenomenon of electrorheology and its applications have been presented by Block and Kelly (1988), and Jordan and Shaw (1989).

In the case of a viscoplastic material, the shear stress $\tau_{xr}(r)$ has to exceed the finite 'yield' stress, τ_y, to initiate flow. This value of the 'yield' stress can be understood as the *capacity* of the material to exist in a solid state. If the stress-demand, $\tau_{xr}(r)$, given by equation (2) exceeds the capacity of the ER material, τ_y, then the ER material adjacent to the walls will yield and flow. For a rigid-viscoplastic material the velocity profiles across these 'fluidized' rings are parabolic whereas the velocity profile across the remaining solid-core ring is constant. From equation (2), one immediately recognizes that as the

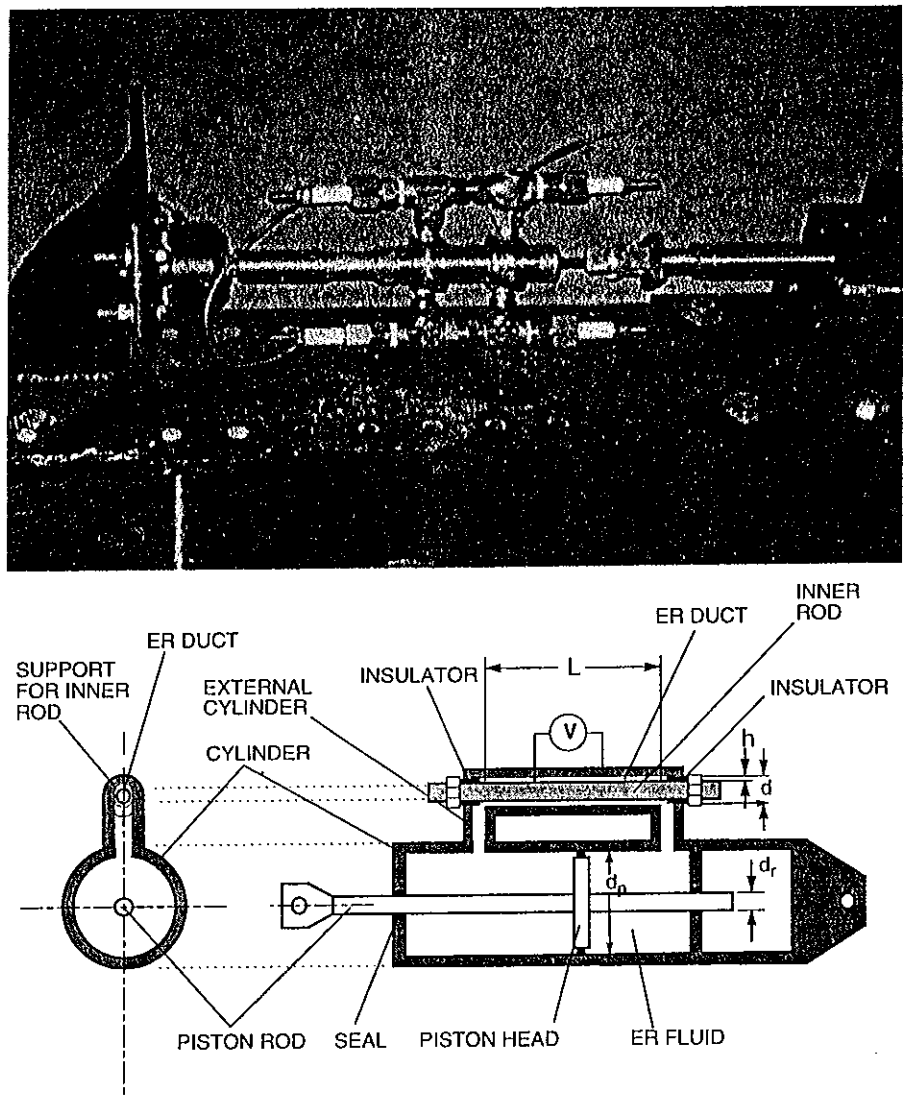

Figure 1. View of the constructed electrorheological damper (top) and a schematic of the proposed electrorheological fluid damper (bottom).

pressure drop increases, more material yields. More on the analysis of viscoplastic Poiseille flow can be found in Phillips (1969). When the stress–strain law of a rigid viscoplastic material is described with the Bingham model,

$$\tau_{xr} = \tau_y \operatorname{sgn}(\dot{\gamma}_{xr}) + \nu_0 \dot{\gamma}_{xr} \tag{5}$$

the pressure drop, Δp, must satisfy (Phillips 1969, Makris *et al* 1996)

$$\Delta p = \frac{12\nu_0 L Q}{\pi d h^2}\left(1 - 3\frac{\tau_y}{\Delta p}\frac{L}{h} + 4\left(\frac{\tau_y}{\Delta p}\right)^3\left(\frac{L}{h}\right)^3\right)^{-1}. \tag{6}$$

Equation (6) is a nonlinear cubic equation in Δp, which can be expressed as

$$\Delta p^3 - \left(3\tau_y\frac{L}{h} + \frac{12\nu_0 L Q}{\pi d h^2}\right)\Delta p^2 + 4\tau_y^3\left(\frac{L}{h}\right)^3 = 0. \tag{7}$$

The solution of the cubic equation given by (7) is available in standard mathematical handbooks (Spiegel 1968). In the limiting case of a purely viscous material ($\tau_y = 0$) equation (7) collapses to (4).

2.3. Flow of elastic-viscoplastic material

The ER fluid used within the damper consists of a carrier which is silicone oil with specific density 0.970, and the suspended solid is zeolite with a concentration of 46% by weight. Oscillatory viscometric tests under the presence of an electric field demonstrated that the silicon-oil–zeolite mixture manifests more pronounced electrorheological properties than a similar mineral-oil-based mixture studied by Gamota and Filisko (1991) and Gamota *et al* (1993). Figure 3 shows recorded stress–strain loops of the silicon-oil–zeolite mixture at different values of the electric field and at frequencies of 1.0, 5.0 and 10 Hz.

The elastic behavior of the material can be clearly observed when the motion reverses direction (see figure 3). For instance, at $E = 3$ kV mm^{-1} the slope of the loop at

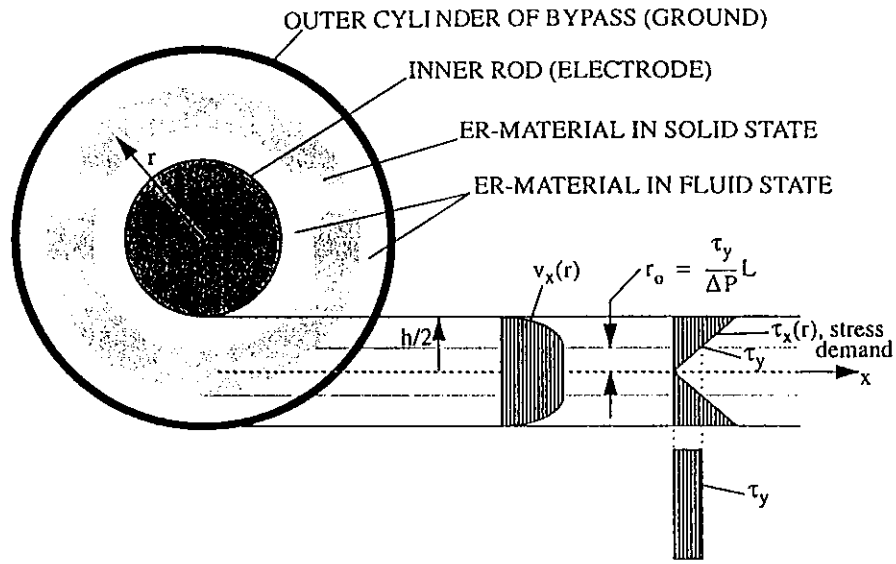

Figure 2. Stress and velocity profiles of the yielding ER fluid across the bypass.

maximum strain is equal to the elastic shear modulus of the material before yielding. In the foregoing analysis where equation (6) was derived, the elasticity of the material before yielding was neglected and the ER fluid was assumed rigid-viscoplastic.

Ehrgott and Masri (1992) and Kamath and Wereley (1996) proposed system identification techniques to capture the elastic-viscoplastic behavior of ER fluids. Recently, a continuum mechanics constitutive model that accounts for the elasto-viscoplastic behavior of the ER fluid has been developed by Makris *et al* (1996):

$$\tau_{xr} + \left[\frac{\eta_0\dot{\gamma}_{xr} + \tau_y\,\mathrm{sgn}(\dot{\gamma}_{xr})}{G\dot{\gamma}_{xr}}\right]\frac{\mathrm{d}\tau_{xr}}{\mathrm{d}t} = \eta_0\dot{\gamma}_{xr} + \tau_y\,\mathrm{sgn}(\dot{\gamma}_{xr}). \tag{8}$$

Equation (8) is a linear first-order equation with variable coefficients, and its analytical solution can be constructed using an integration factor. It is recalled that the differential equation

$$\frac{\mathrm{d}\tau(t)}{\mathrm{d}t} + R(t)\tau(t) = Q(t) \tag{9}$$

has the solution

$$\tau(t) = \mathrm{e}^{-\int R(t)\mathrm{d}t}\left[\int_{-\infty}^{t} Q(\xi)\mathrm{e}^{\int R(\xi)\mathrm{d}\xi}\mathrm{d}\xi + C\right]. \tag{10}$$

The solution of (8) can also be expressed in the form of (10). For a harmonic strain-rate-induced excitation, $\dot{\gamma}_{xr}(t) = \omega\gamma_0\cos\omega t$, the exponent, $\int R(t)\mathrm{d}t$, in (10), for $-\pi/2 \le \omega t \le \pi/2$ is given by

$$\int \frac{G\omega\gamma_0\cos\omega t}{\eta_0\omega\gamma_0\cos\omega t + \tau_y}\mathrm{d}t$$

$$= \begin{cases} \dfrac{G}{\eta_0\omega}\left[\omega t - \dfrac{2a}{\sqrt{a^2-1}}\,\mathrm{atan}\dfrac{\sqrt{a^2-1}\tan(\omega t/2)}{a+1}\right] \\ \qquad a^2 > 1 \\ \dfrac{G}{\eta_0\omega}[\omega t - \tan(\omega t/2)] \\ \qquad a = 1 \\ \dfrac{G}{\eta_0\omega}\left[\omega t - \dfrac{a}{\sqrt{1-a^2}}\ln\dfrac{\sqrt{\frac{1+a}{1-a}} + \tan(\omega t/2)}{\sqrt{\frac{1+a}{1-a}} - \tan(\omega t/2)}\right] \\ \qquad a^2 < 1 \end{cases} \tag{11}$$

in which $a = \tau_y/\eta_0\omega\gamma_0$. For the case where $\pi/2 \le \omega t \le 3\pi/2$, the dimensionless quantity, a, has to be replaced by $-a$, and the symmetric part of the response is obtained.

For the expressions of the integration-factor-exponent given by (11), a closed form solution of (10) is not known to the authors. Nevertheless, equation (10) can be integrated numerically. Figure 3 compares the predictions of the proposed model at three different frequencies (f = 1 Hz, 5 Hz and 10 Hz) of the induced strain-rate excitation. The comparison is very encouraging. The values of the yield stress, τ_y(3 kV mm^{-1} = 0.26 psi (1.8 kPa), elastic shear modulus, G = 2.46 psi (17 kPa), and field-dependent zero-shear-rate viscosity, η_0(3 kV mm^{-1} = 0.0019 psi s (13 Pa s).

Figure 4 (top) shows the response of the model at the zero frequency limit. The results obtained with the numerical integration of (10) with a = 2000 are compared with the closed form solution of (10), which is known when $a = \infty$ (Makris *et al* 1996). The results obtained with the two solutions are almost identical. Figure 4 (bottom) also depicts the model prediction at high frequencies ($a^2 \ll 1$). The shape of the loop (solid line) suggests that at the high-frequency limit, the response of the model is linear viscoelastic. In fact, as frequency increases, the model of (8) reduces to the classical linear Maxwell model. This can

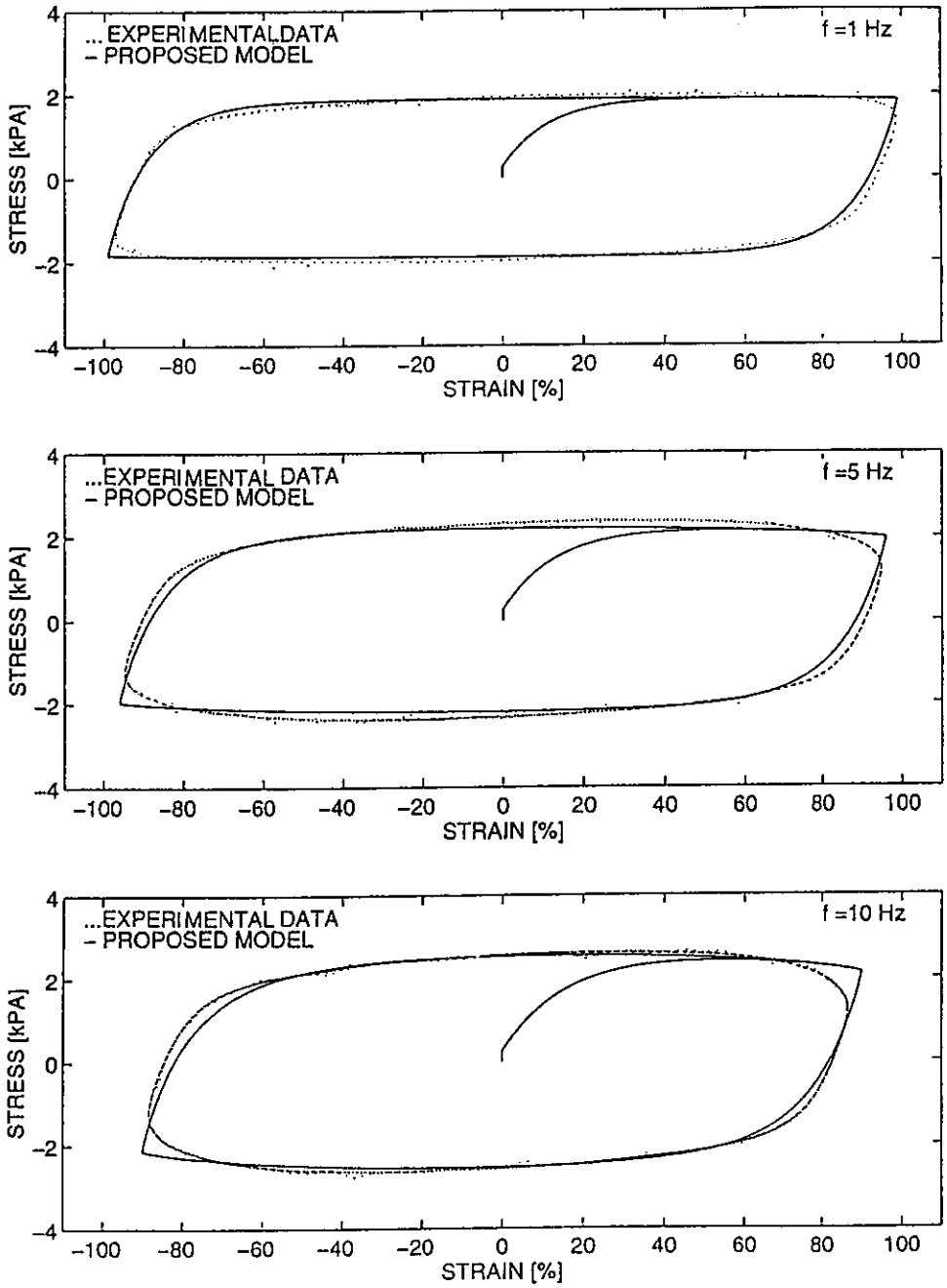

Figure 3. Comparison of recorded and predicted stress–strain loops of the ER fluid at different frequencies and an electric field of 3 kV mm^{-1}. Dashed lines: experimental data. Solid lines: prediction of proposed model (equation (8)). 1 psi = 6.89 kPa.

be shown by observing equation (11). At high frequencies ($a^2 \ll 1$) equation (11), reduces to

$$\int \frac{G\omega\gamma_0 \cos \omega t}{\eta_0 \omega \gamma_0 \cos \omega t + \tau_y} \, dt = \frac{G}{\eta_0 \omega}\left[\omega t - a \ln \frac{1 + a + \tan(\omega t/2)}{1 + a - \tan(\omega t/2)}\right] \tag{12}$$

for $a^2 \ll 1$ and $-\pi/2 \leq \omega t \leq \pi/2$. The largest value of the argument of the logarithm in (12) is when $\omega t = \pi/2 \Rightarrow \tan(\omega t/2) = 1$. At this limit the second term within the square brackets in (12) becomes $a \ln(2 + a)/a$ which tends to zero as a tends to zero. Accordingly, as $a \to 0$ then

$$\int \frac{G\omega\gamma_0 \cos \omega t}{\eta_0 \omega \gamma_0 \cos \omega t + \tau_y} \, dt \to \frac{G}{\eta_0} t$$

and equation (10) becomes the linear Maxwell model (Bird *et al* 1987):

$$\tau(t) = e^{-(G/\eta_0)t} \int_{-\infty}^{t} G\dot{\gamma}(\xi) e^{(G/\eta_0)\xi} \, d\xi. \tag{13}$$

Figure 4 (bottom) compares the prediction of the proposed

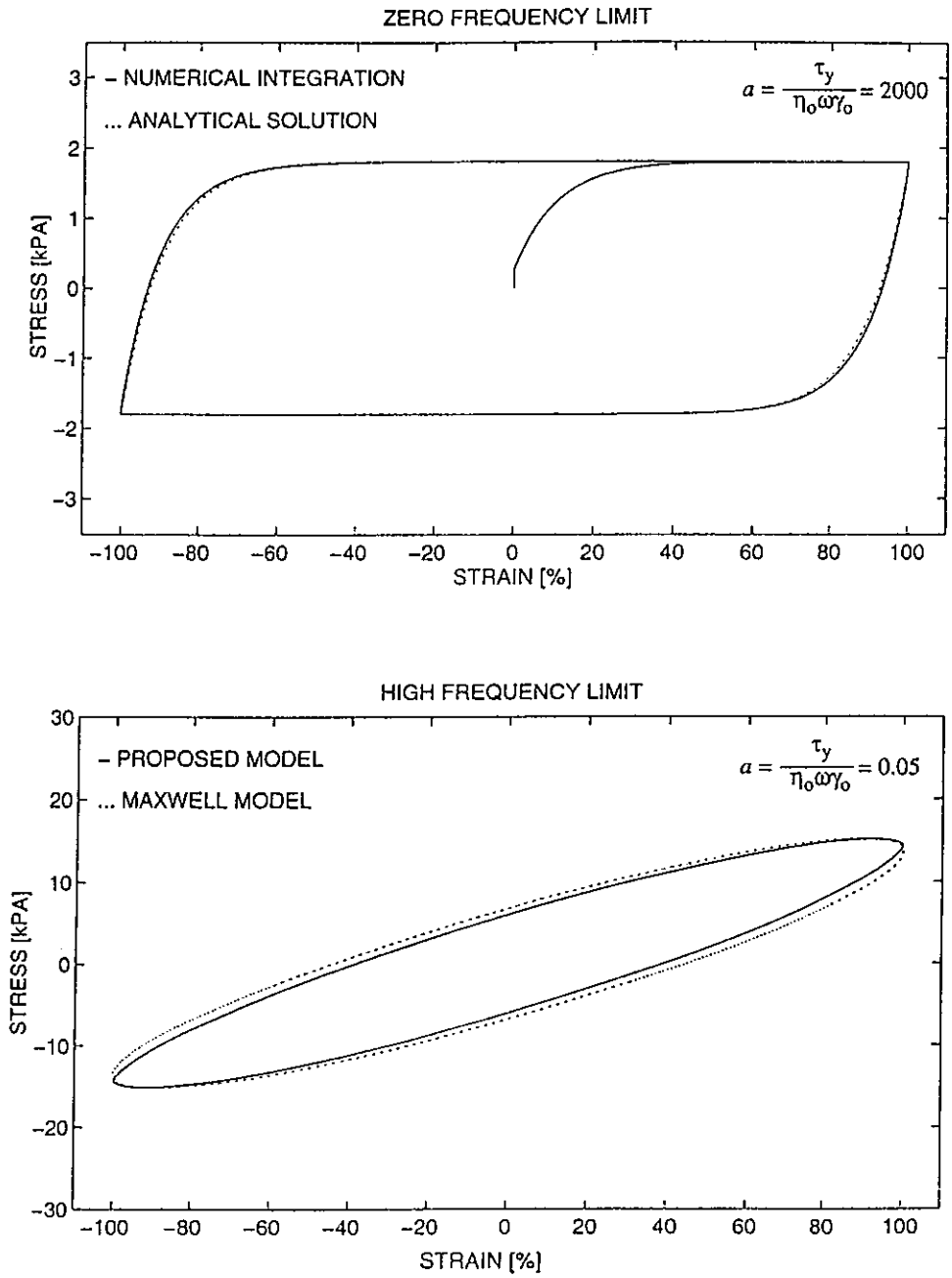

Figure 4. Behavior of the proposed constitutive model at the low (top) and high (bottom) frequency limits. 1 psi = 6.89 kPa.

model for the value of $a = 0.05$ with the prediction of the Maxwell model given by (13). The two responses are almost identical. Consequently, the model given by equation (8) captures the ER fluid response at all frequencies. However, a closed-form solution for the pressure drop, when the stress–strain law is described by (8) is not known to the authors. Nevertheless, numerical studies show that the elasticity of the material plays a negligible role in the macroscopic response of the damper and equation (5) (rigid-viscoplastic behavior) can be used instead of the more realistic equation (8) (elastic-viscoplastic behavior).

3. Experimental program and response prediction

Dynamic testing of the damper was conducted using the arrangement shown in figure 1 (top). A hydraulic actuator imposes a prescribed displacement history along the axis of the damper. The force developed in the damper is measured through a stationary load cell which is connected between the damper and the reaction frame (left end on figure 1). The displacement of the damper is measured using an LVDT (linear variable differential transducer) which is located within the actuator.

The electric field on the ER duct is applied through the cathode connected at the right end of the inner cylinders

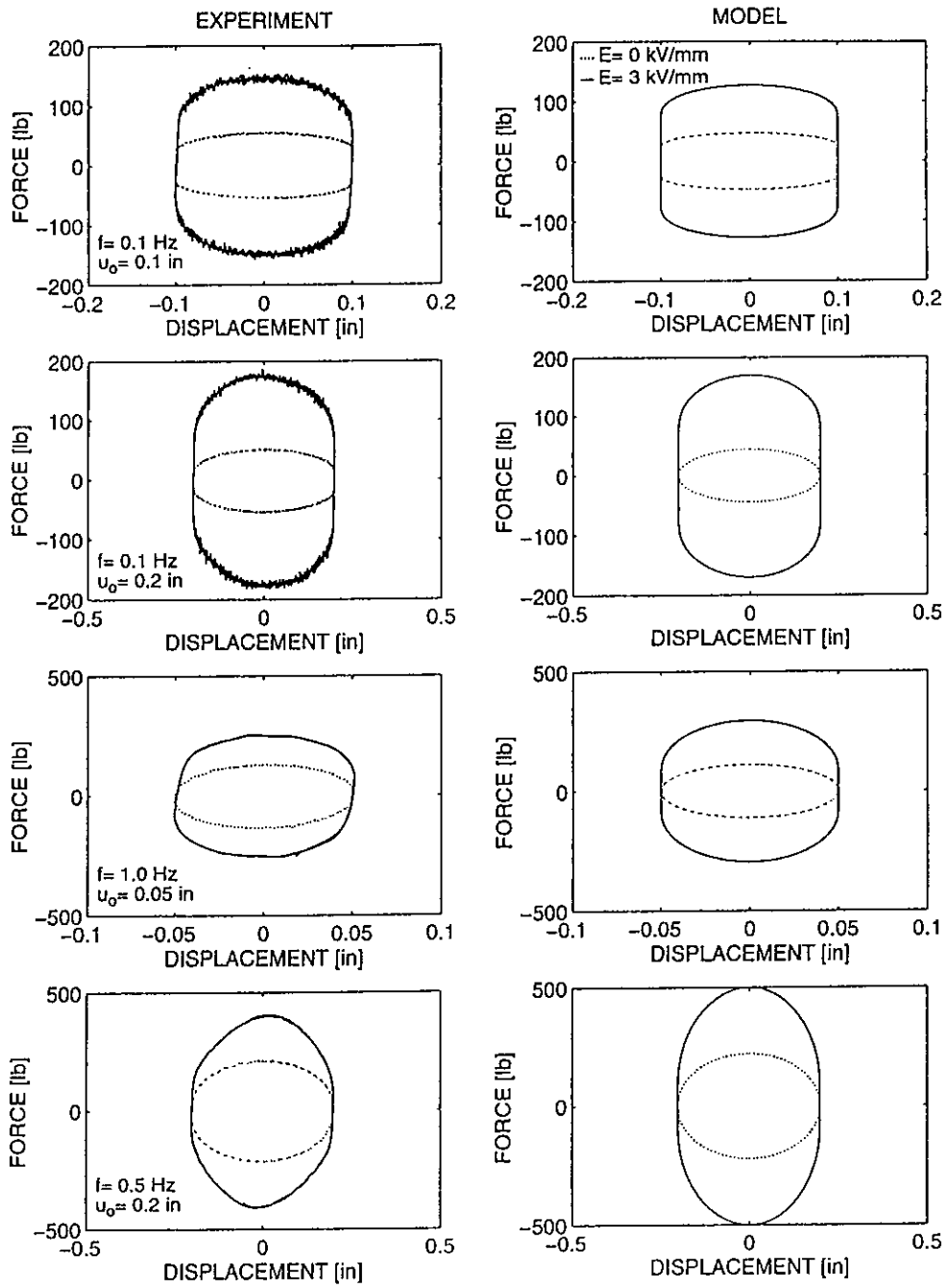

Figure 5. Comparison of recorded and predicted force–displacement loops of the electrorheological damper with and without electric field (1 lb = 4.448 N, 1 in = 25.4 mm).

of the bypasses shown in figure 1 (top). The other wire shown on figure 1 is connected to a temperature transducer to monitor the temperature of the fluid along the bypass. This temperature exceeds the temperature of the cylinder of the damper, since fluid velocities along the bypass are larger. The recorded temperature should not exceed approximately 240 °C (450 °F) to prevent damaging the insulators. The recorded temperature during experiments ranging from 75 °F to 85 °F. The maximum current that we measured during the experiments was of the order of 0.5 mA and the resulting maximum power needed from the ER damper is less than 1.0 W.

Figure 5 shows recorded (left) and predicted (right) force–displacement loops without electric field ($E = 0$) and with $E = 3$ kV mm^{-1}. At zero electric field, the recorded loops are nearly elliptical, whereas at $E = 3$ kV mm^{-1} some nonlinear behavior becomes apparent. As the piston velocity increases, viscous effects dominate over plastic effects, and the fraction of the force that can be controlled is reduced.

The predicted loops shown on the right of figure 5 are

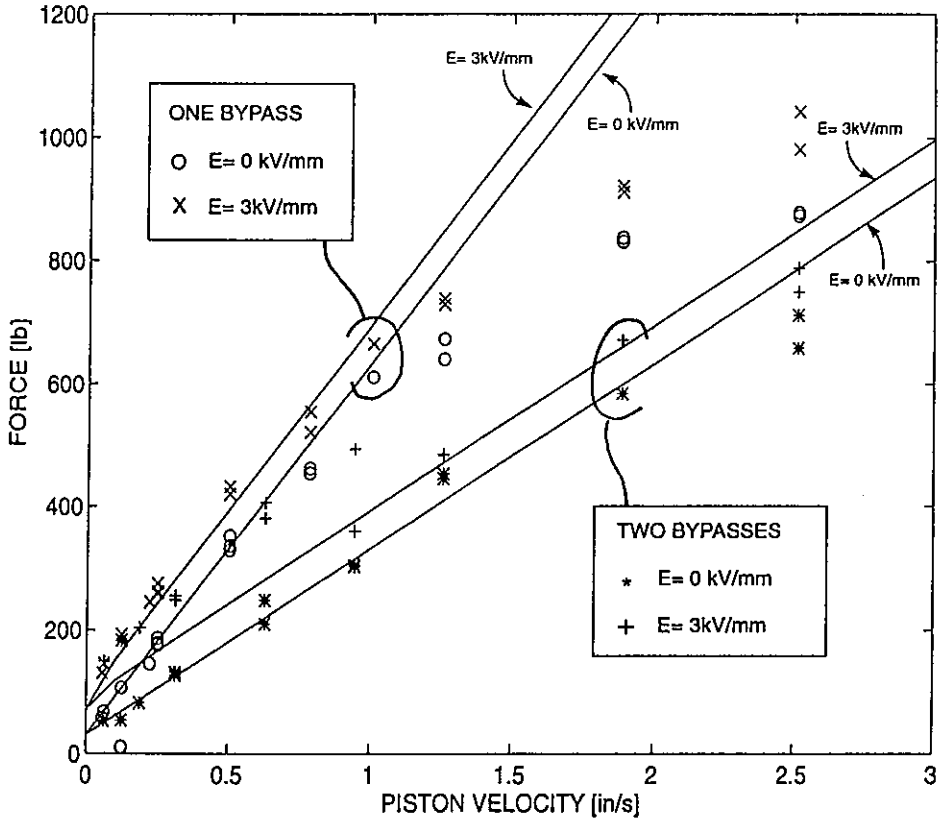

Figure 6. Comparison of recorded amplitudes of piston forces as a function of maximum piston velocity from harmonic oscillatory tests.

computed with the equation

$$P(t) = \Delta p(t)A_p + P_y \mathrm{sgn}[\dot{u}(t)] \qquad (14)$$

where $P_y = 25$ lbs (112 N) is a permanent friction force exerted on the piston rod from the damper seals and A_p is the area of the piston head. $\Delta p(t)$ is the pressure drop across the piston head. Herein the pressure drop was computed using equation (7) which is based on the approximate rigid-viscoplastic model given by (5). The value of the yield stress used in equation (7) is the value that was obtained from the oscillatory viscometric tests, $\tau_y(3\ \mathrm{kV\ mm^{-1}}) = 0.26$ psi (1.8 kPa). At $E = 0$, $\tau_y = 0$ and the value of the zero-shear-rate viscosity used is $\eta_0 = 0.001$ psi s (7 Pa s). When the electric field is present the value of the viscosity at $E = 3$ kV mm^{-1}, $\eta_0 = 0.0019$ psi s (13 Pa s), was used.

Figure 6 shows the amplitudes of recorded force versus piston-velocity amplitudes at zero field, (O) and at $E = 3$ kV mm^{-1} (×). The scatter in the data is due to viscous heating during testing. As the harmonic tests were conducted one after the other the damper was subjected to many cycles and in some tests the temperature along the bypass was higher than during others (ranging from 75 °F to 85 °F). At zero field and small piston velocities the damper operates like an ideal dashpot ($F(t) = C(\mathrm{d}u/\mathrm{d}t)$), where C is the small-velocity damping constant which can be computed from

$$C = \frac{12\eta_0 L}{\pi d h^3} A_p^2 \qquad (15)$$

where A_p is the piston-head area. With reference to figure 1 the geometric characteristics of the constructed damper are: $L = 2.15$ in (54.6 mm), $d = 0.563$ in (14.3 mm), $h = 0.0315$ in (0.8 mm), $d_p = 1.315$ in (33.4 mm), $d_r = 0.443$ in (11.25 mm). Using these values and with $\eta_0 \approx 0.001$ psi s (7 Pa s), equation (15) yields a value of $C = 690$ lb s in^{-1} (120 kN s m^{-1}). This value is close to the slope of the solid line shown on figure 6 for one bypass and indicates that the Hagen–Poiseuille theory predicts well the damper response for piston velocities less than 0.6 in s^{-1}. The finite value of the force at zero velocity and $E = 0$ is due to the friction force that the seals exert on the rod.

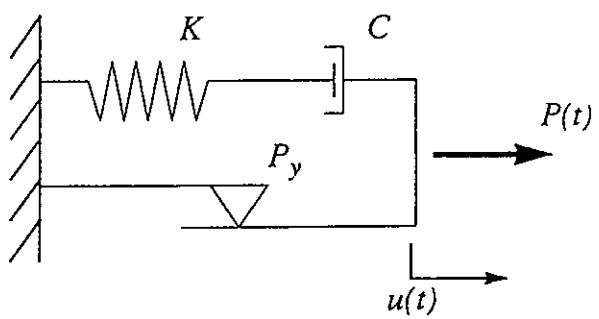

Figure 7. Schematic of the BingMax model.

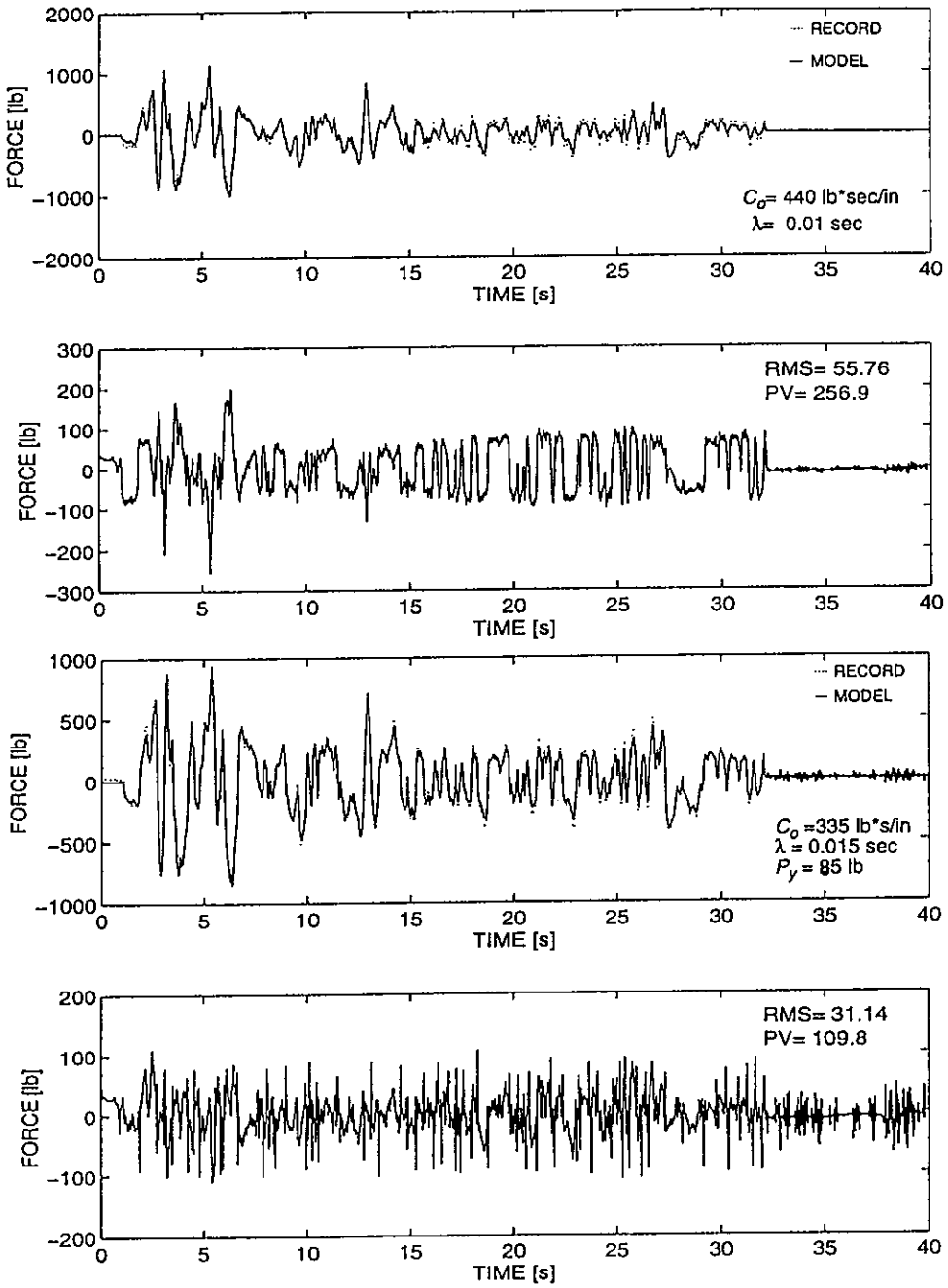

Figure 8. Comparison of recorded and predicted forces and difference signals at $E = 3$ kV mm^{-1} of the Maxwell model (top 2 plots) and the BingMax model (bottom 2 plots).

At higher piston velocities the damper delivers a force proportional to the velocity raised to a power which is less than one ($F(t) = C(\mathrm{d}u/\mathrm{d}t)^{\alpha}$, $0 < \alpha < 1$). This desirable behavior is achieved because at high piston velocities some fluid flows between the piston head and the main cylinder.

4. Macroscopic modeling of the damper response

Modeling the response of semi-active dampers is a key issue in the design and implementation of these devices in civil structures. Structural control engineers are primarily interested in macroscopic models that describe the response of the damper at the force–displacement level. Macroscopic models can vary from physically motivated mechanical models to nonparametric models used for pattern recognition or function approximation (e.g. artificial neural networks). The problem of developing a macroscopic model that predicts the response of a structural or mechanical system does not have a unique solution. Poincaré (1929) pointed out that if a physical phenomenon can be represented by one mechanical model it can be represented by many other models. Thus 'springs', 'dashpots' and 'sliders' could be arranged in many different

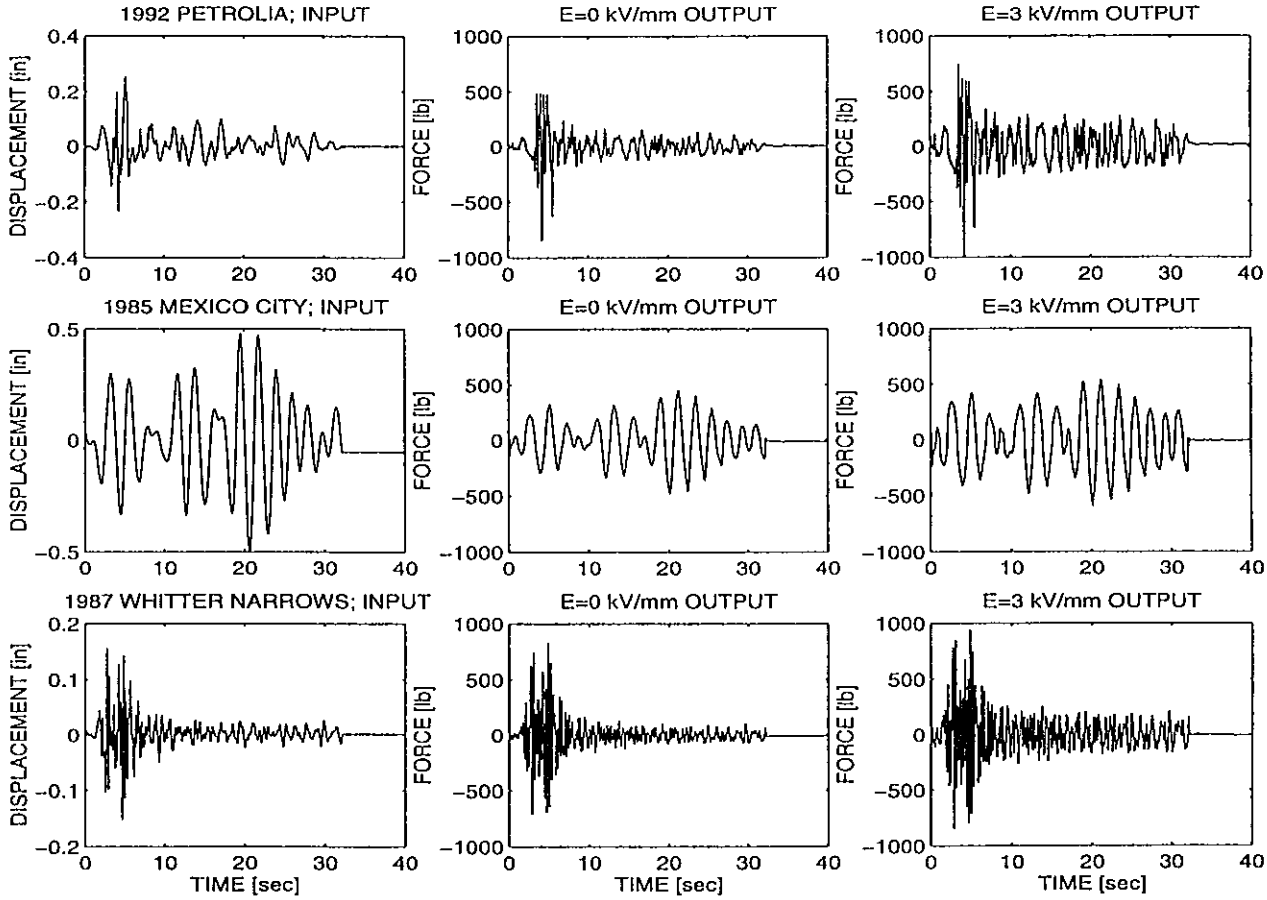

Figure 9. Recorded input–output signals used to train the neural network at $E = 0$ and $E = 3$ kV mm^{-1}.

patterns with all of them being equivalent (Shames and Cozzarelli 1992).

4.1. Phenomenological models

The challenge in modeling the response of semi-active dampers is to capture satisfactorily both nonlinear and frequency-dependent effects. Burton (1996) studied in detail the performance of standard phenomenological models, such as the Bingham model, the Maxwell model and a combination of these two models, named the BingMax model, which is schematically shown in figure 7.

Herein, it is shown that the BingMax model captures satisfactorily both hysteretic and frequency-dependent behavior. The constitutive law of the BingMax model shown on figure 7 can be expressed as

$$P(t) = K \int_0^t e^{-(t-\tau)/\lambda} \dot{u}(\tau)\, d\tau + P_y \operatorname{sgn}[\dot{u}(t)]. \qquad (16)$$

The top plot in figure 8 compares the prediction of a calibrated standard Maxwell model with the recorded force from the damper when subjected to the 1940 El Centro displacement history. The second plot on figure 8 shows the difference signal between the recorded and predicted signal with a peak value of PV = 257 lb and a root mean square value of RMS = 56 lb. The third plot on figure 8 compares the prediction of the BingMax model given by (16) with the recorded force from the damper when subjected to the 1940 El Centro displacement history; the bottom plot on figure 8 shows the difference signal between the recorded and predicted signal with PV = 109 lb and an RMS = 31.14 lb. Clearly, the BingMax model outperforms the Maxwell model.

4.2. Neural network models

Neural networks are useful as models of nonlinear dynamical systems because of their ability to be universal function approximators. Several types of neural network appear to offer promise for use in function approximation. These include the multi-layer neural network trained with the back-propagation algorithm commonly attributed to Rumelhart *et al* (1986), the recurrent neural network such as the feedback network of Hopfield (1982), the content-addressable memory of Kohonen (1980), and the Gaussian node network of Moody and Darken (1989). The choice of which neural network to use and which training procedure to invoke is an important decision and varies depending on the intended application. It has been shown that feedforward neural networks can approximate arbitrarily well any continuous function; this, in fact, can

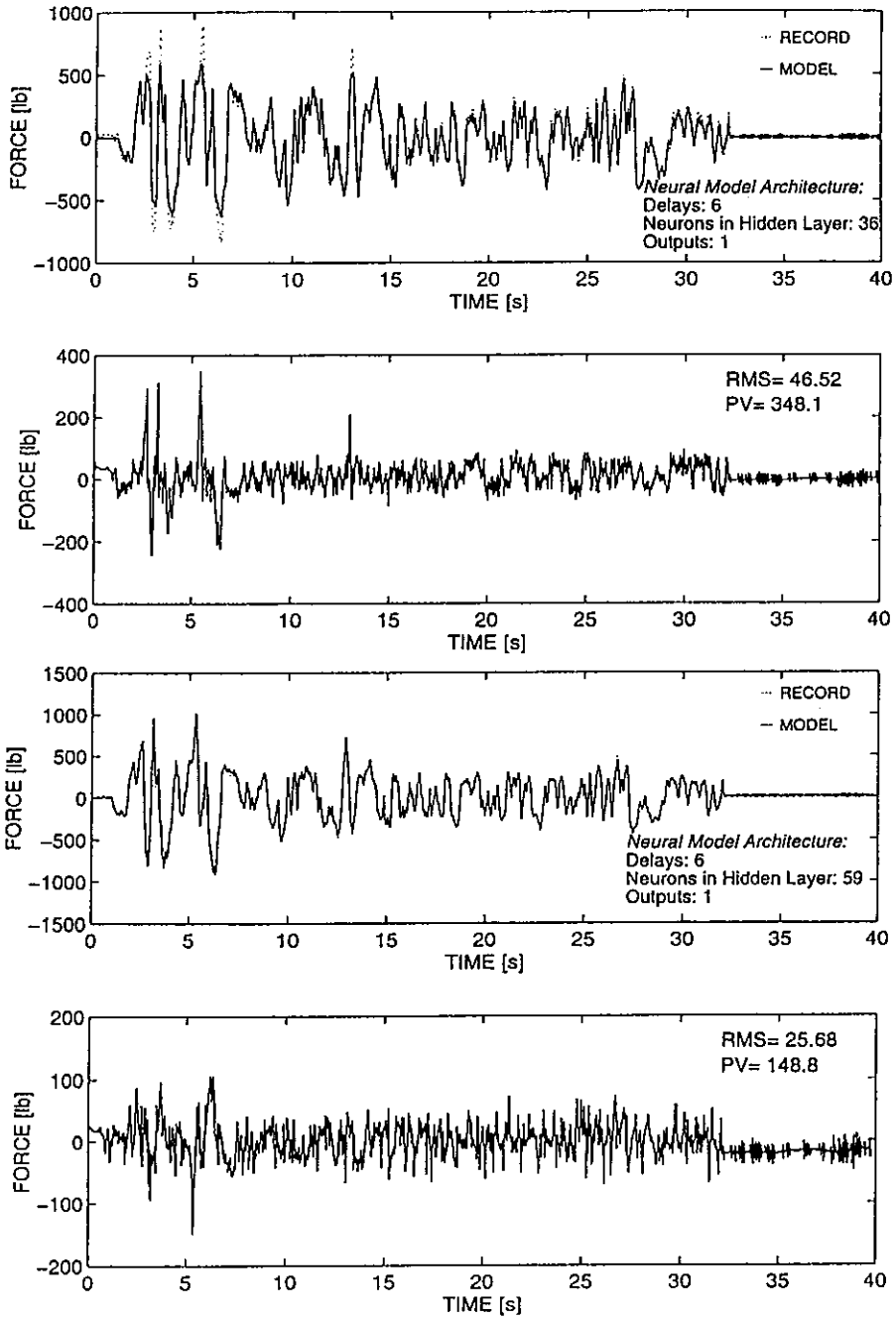

Figure 10. Comparison of recorded and predicted forces and difference signals at $E = 3$ kV mm^{-1} of the neural network model (top 2 plots) and the combined model (bottom 2 plots).

be accomplished using a feedforward network with a single hidden layer of neurons and a linear output unit.

Herein, the Dependence Identification Algorithm (DIA) (Moody and Antsaklis 1995) is utilized to construct and train a multilayer neural network to predict the response of the electrorheological damper. The DIA bears some similarities to the boolean network construction algorithm, however it is designed to work with continuous training problems and it uses the concept of linear dependence, instead of the desired boolean output value, to group patterns together. The algorithm does not share the problems of network pruning techniques because it builds from a small network up to a large one, and because it does not use gradient descent. The DIA is an extremely fast algorithm for function approximation with the advantage that it generates an appropriate network, thus eliminating the need for experimentation to determine the number of hidden neurons. The DIA creates a network and sets of initial conditions which are suitable for further iterative or on-line adaptive training with gradient techniques such as back-propagation.

The DIA utilizes displacement-force input–output pairs

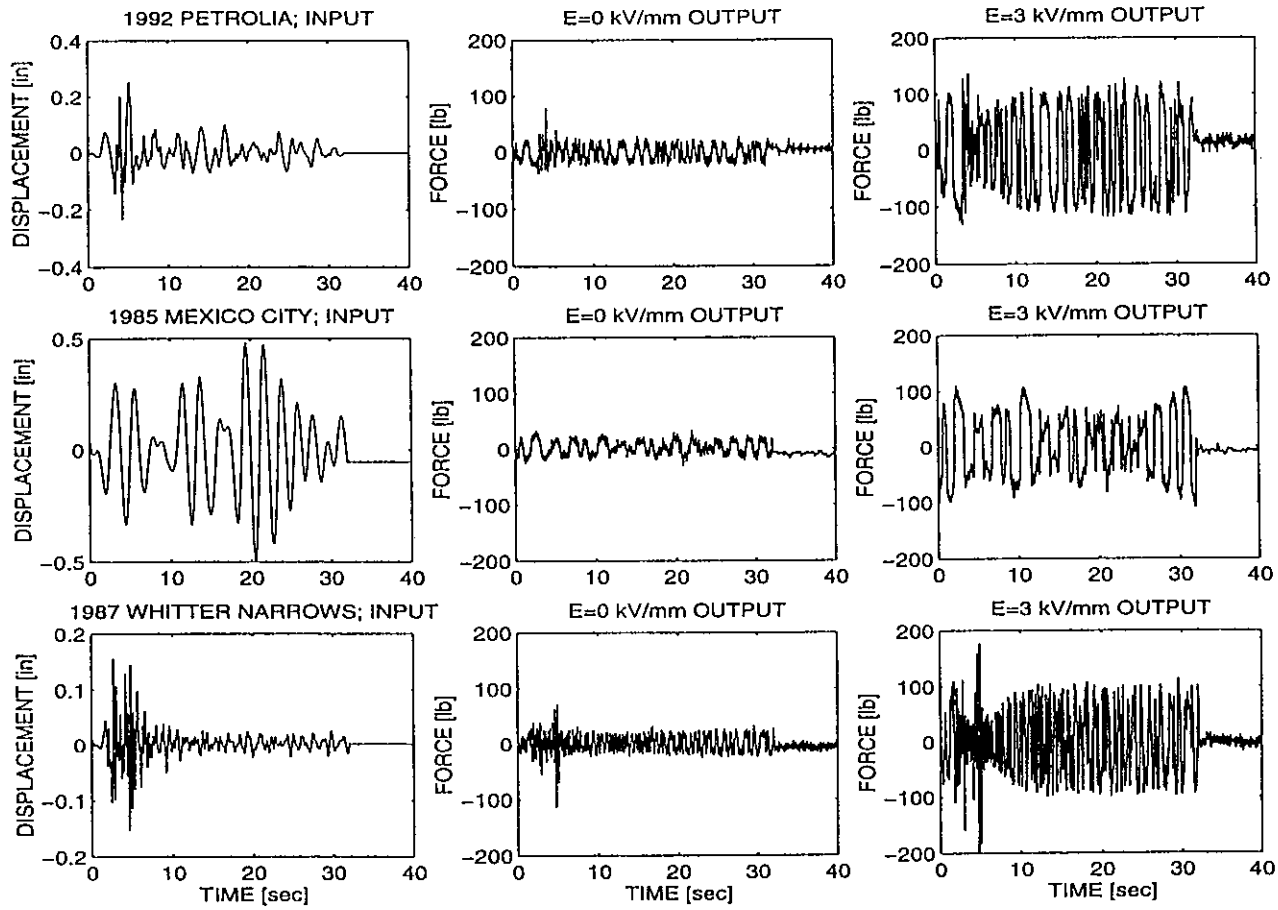

Figure 11. Recorded input–output signals used to train the combined model at $E = 0$ and $E = 3$ kV mm^{-1}.

recorded in the laboratory to construct and train the neural network. The neural networks are single hidden layer networks with seven inputs, 99 neurons, one output and six delays. Displacement histories from three earthquakes have been used as an input to the fluid damper. The three input seismic records used are the 1985 Mexico City earthquakes, the 1987 Whittier Narrows earthquake (Tarzana record) and the 1992 Petrolia earthquake which are shown on the left of figure 9. The resultant force needed to maintain the motion was recorded with the load cell shown on figure 1. Figure 9 (center) plots the corresponding recorded forces when $E = 0$ and figure 9 (right) plots the corresponding recorded forces when $E = 3$ kV mm^{-1}.

Figure 10 (top) compares the prediction of the trained neural network with the experimentally measured force. The agreement is acceptable, but both the peak value, PV = 348 lb, and the root mean square, RMS = 47 lb, of the resulting different signal are larger than the corresponding values resulting from the phenomenological BingMax model shown at the bottom of figure 8. Similar results have been obtained for the case where $E = 0$.

4.3. Combined model

Modeling of the damper can be improved by combining phenomenological models with a neural network. The philosophy advanced herein is that a simple phenomenological model will capture most of the linear response of the ER damper and the neural network will approximate the inherent nonlinear behavior of the ER damper resulting from the yielding of the fluid together with additional nonlinearities originating from the frictional behavior at the attachments of the ER damper. Initially, we investigated the case where the neural network was trained on the difference signal between the prediction of the BingMax model and the recorded force history. However, since the BingMax model captures most of the nonlinear response, the difference signal was practically a noise with virtually no coherence, and the DIA did not converge. In contrast, when the neural network was trained on the difference signal between the prediction of the Maxwell model and the recorded force history, the DIA converged. Figure 11 shows the input–output training pairs used to generate the neural network architecture and back-propagation for $E = 0$ (center) and $E = 3$ kV mm^{-1} (right). The number of neurons used in the hidden layers are shown on figure 10 (bottom). Figure 10 (bottom) shows the difference signal between the prediction from the combined model and the recorded response. Both peak values and root mean squares are improved when compared with all other models. Finally, figure 12 shows the performance of the combined model when predicting harmonic responses at different frequencies ($F = 0.5$, 2.0 and

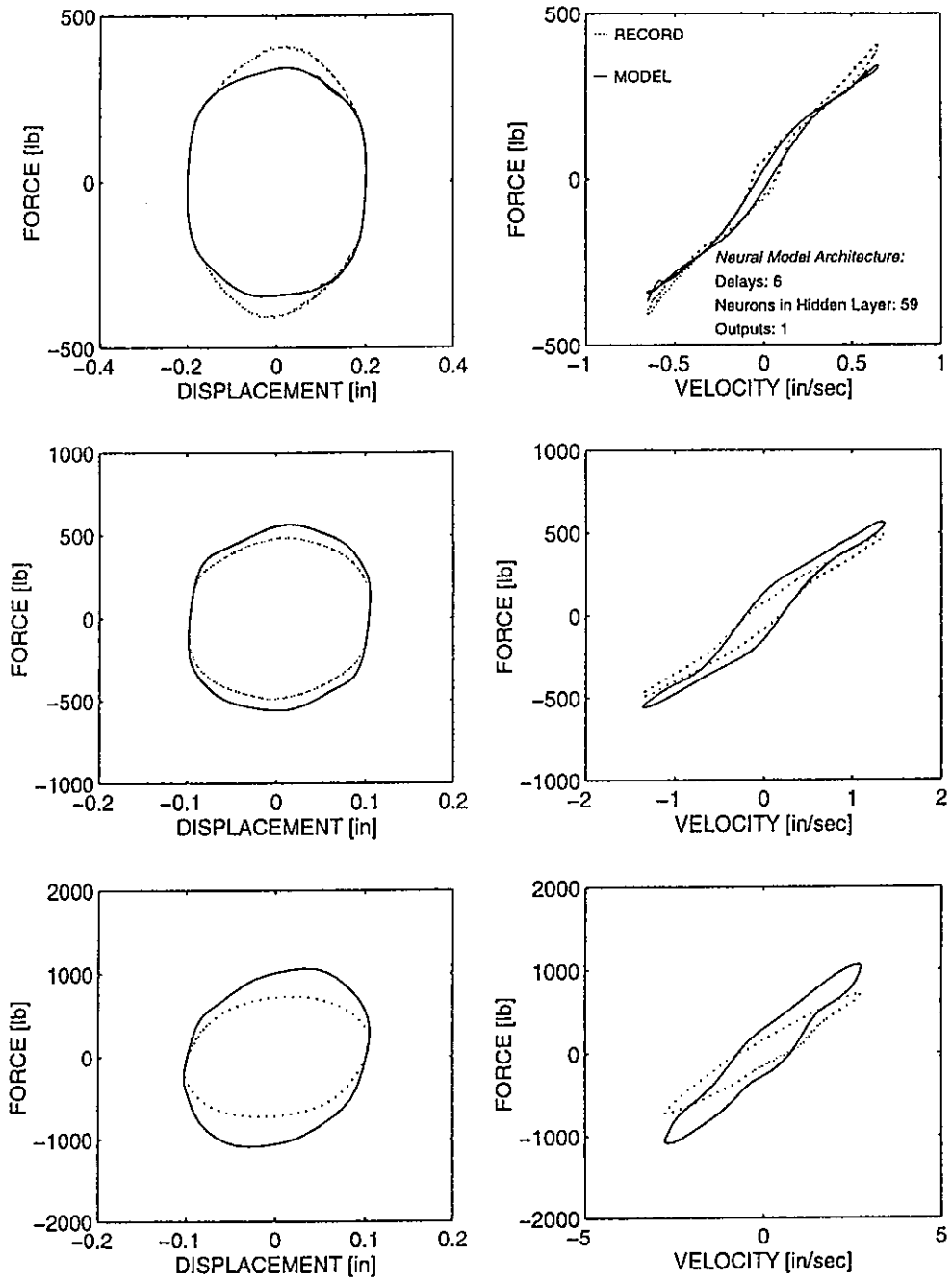

Figure 12. Comparison of recorded and predicted force–displacement and force–velocity loops at $E = 3$ kV mm^{-1}. Solid line: combined Maxwell model with neural network; dashed line: recorded motion. Top: $f = 0.5$ Hz; center: $f = 2.0$ Hz; bottom: $f = 4$ Hz.

4.0 Hz) . The performance is encouraging since the neural network has only been trained to earthquake motions.

5. Conclusions

In this paper the mechanical behavior of a silicon-oil-based ER fluid and the flow across a cylindrical duct of an ER damper developed for seismic protection applications are analysed. The developed damper consists of an outer cylinder and a piston rod that pushes the ER fluid through a stationary annular duct. The ER fluid used in the damper manifests viscosity, plasticity and elasticity. An elastic-viscoplastic law at the stress–strain level has been proposed that predicts satisfactorily the fluid behavior at different deformation rates. The flow of the ER fluid through the bypass can be approximated with the Hagen–Poiseille flow theory, and a dependable formula was derived which relates the pressure drop to the piston velocity, the physical properties of the fluid and the size of the damper. Subsequently, the performance of physically motivated phenomenological models and neural networks

has been examined when predicting the measured response of the ER damper. It was found that a neural network constructed with the Dependence Identification Algorithm when combined with a standard Maxwell model predicts satisfactorily the response of the damper with and without the presence of electric field.

Acknowledgments

Partial support for this work has been provided by the National Science Foundation, Grant BCS-9300827, and by the Graduate School of the University of Notre Dame. The main cylinder of the damper was manufactured and donated by Taylor Devices, Inc., N Tonawanda, NY. Professor D Hill and Ms M Jordan manufactured the ER fluid. Special thanks to Mr Richard Strebinger for helping in the construction of the ER bypass and to Mr J Moody for helping with the Dependence Identification Algorithm.

References

ATC-17-1 1993 *Proc. Seminar on Seismic Isolation, Passive Energy Dissipation, and Active Control* vol 1&2 (Applied Technology Council)

Bird B, Armstrong R and Hassager O 1987 *Dynamics of Polymeric Liquids* (New York: Wiley)

Block H and Kelly J P 1988 Electrorheology *J. Appl. Phys.* **21** 1661–77

Burton S A 1996 Design and analysis of an electrorheological damper for seismic protection of structures *MS Thesis* University of Notre Dame, IN

Burton S A, Makris N, Konstantopoulos I and Antsaklis P J 1996 Modeling the response of an electrorheological damper: phenomenology and emulation *J. Eng. Mech. ASCE* **122** at press

Constantinou M C and Symans M D 1993 Seismic response of structures with supplemental damping *Struct. Design Tall Build.* **2** 77–92

Duclos T G 1988 Electrorheological fluids and devices *Automotive Eng.* **96** 45–8

Ehrgott R C and Masri S F 1992 Modeling the oscillatory dynamic behavior of electrorheological materials in shear *Smart Mater. Struct.* **1** 275–85

Gamota D R and Filisko F E 1991 Dynamic mechanical studies of electrorheological materials: moderate frequencies *J. Rheology* **35** 399–425

Gamota D R, Wineman A S and Filisko F E 1993 Fourier transform analysis: nonlinear dynamic response of an electrorheological material *J. Rheology* **37** 919–33

Gavin H P and Hanson R D 1994a Characterization of an ER active member *Proc. Structures Congress XII (Atlanta, GA)* ed Baker and Goodno vol 2, pp 863–8

Gavin H P and Hanson R D 1994b Electrorheological dampers for structural vibration suppression *Report No. UMCEE 94-35* Department Civil and Environmental Engineering, University of Michigan, Ann Arbor, MI

Hopfield J J 1982 Neural networks and physical systems with emergent collective computational abilities *Proc. National Academy of Science, USA* **79** 2554–8

Housner G W, Soong T T and Masri S F 1994 Second generation of active structural control in civil engineering *Proc. First World Conf. on Structural Control (Los Angeles, CA)* vol 1, pp 3–18

Jordan T C and Shaw M T 1989 Electrorheology *IEEE Trans. Electron. Insulation* **24** 849–78

Kamath G M and Wereley N M 1995 A nonlinear viscoelastic-plastic model for electrorheological fluids *Smart Mater. Struct.* to appear

Kawashima K and Unjoh S 1994 Seismic response control of bridges by variable dampers *J. Struct. Eng.* **120** 2583–601

Kohonen T 1980 *Content-Addressable Memories* (New York: Springer)

Makris N, Burton S, Hill D and Jordan M 1996 Analysis and design of an electrorheological damper for seismic protection of structures *J. Eng. Mech. ASCE* **122** at press

Masri S F, Ghassiakos A G and Caughey T K 1993 Identification of nonlinear dynamic systems using neural networks *J. Appl. Mech.* **60** 123–33

Moody J O and Antsaklis P J 1995 The dependence identification neural network construction algorithm *IEEE Trans. on Neural Networks*

Moody J O and Darken D J 1989 Fast learning in networks of locally-tuned processing units *Neural Comput.* **1** 281–94

Müller W 1936 Zum Problem der Anlaufstromung einer Flussigkeit im geraden Rohr mit Kreisring- und Kreisquerschnitt *ZAMM* **16** 227–38 (in German)

Patten W N, Sack R L and He Q 1994 Suppression of vehicle-induced bridge vibration via a semiactive structural controller *Proc. First World Conf. on Structural Control (Los Angeles, CA)*

Poincaré H 1929 The foundation of science *Science*

Phillips R W 1969 Engineering applications of fluids with variable yield stress *PhD Dissertation* University of California, Berkeley, CA

Rumelhart D E, Hinton G E and Williams R J 1986 Learning internal representations by error propagation *Parallel Distributed Processing: Explorations in the Microstructure of Cognition, Vol 1: Foundation* ed Rumelhart and McClelland (Cambridge, MA: MIT Press) pp 318–62

Shames I H and Cozzarelli F A 1992 *Elastic and Inelastic Stress Analysis* (Englewood Cliffs, NJ: Prentice Hall)

Spiegel M R 1968 *Mathematical Handbook of Formulas and Tables (Schaum's Outline Series)* (New York: McGraw-Hill)

Stanway R, Sproston J L and El-Wahed A K 1996 Applications of electrorheological fluids in vibration control: a survey *J. Smart Mater. Struct.* to appear

Symans M and Constantinou M C 1995 Development and experimental study of semi active fluid damping device for seismic protection of structures *Report NCEER-950011* National Center for Earthquake Engineering Research, Buffalo, NY

Winslow W M 1949 Induced vibration of suspensions *Appl. Phys.* **20** 1137–40